Energy & Environmental Science

PAPER

View Article Online
View Journal | View Issue

Cite this: *Energy Environ. Sci.*, 2015, **8**, 1493

Positive onset potential and stability of Cu_2O-based photocathodes in water splitting by atomic layer deposition of a Ga_2O_3 buffer layer†

Changli Li,[a] Takashi Hisatomi,[b] Osamu Watanabe,[b] Mamiko Nakabayashi,[c] Naoya Shibata,[c] Kazunari Domen[b] and Jean-Jacques Delaunay*[a]

Received 24th January 2015,
Accepted 6th March 2015

DOI: 10.1039/c5ee00250h

www.rsc.org/ees

The Cu_2O-based photocathode is considered as one of the most promising photocathodes for high performance water splitting under sunlight. However, the relatively negative onset potential for H_2 production of these photocathodes impedes further optimization of the solar-to-fuel conversion efficiency. Here, a thin Ga_2O_3 buffer layer is introduced between the Cu_2O absorber layer and the TiO_2 protective layer by atomic layer deposition to increase the photovoltage. For the optimized TiO_2 deposition temperature, the Pt/TiO_2/Ga_2O_3/Cu_2O electrode achieves a high cathodic photocurrent of -2.95 mA cm^{-2} at 0 V *vs.* RHE and an extremely positive onset potential of 1.02 V *vs.* RHE (defined as the potential where photocathodic current reaches 20 μA cm^{-2} under air-mass 1.5 global illumination), benefiting from a buried p–n junction and a favorable band alignment. The Pt/TiO_2/Ga_2O_3/Cu_2O electrodes exhibit a stable cathodic current for 2 h under continuous illumination of a 500 W Xe lamp for the TiO_2 deposition temperatures below 180 °C.

Broader context

The photoelectrochemical (PEC) water splitting using sunlight offers a sustainable means to produce hydrogen without relying on any fossil fuels. Cu_2O is one of the most promising photocathode materials with respect to cost, abundance, light absorption, and energy band position, although the application of Cu_2O is limited because of a negative onset potential and self-reduction in the electrolyte under illumination. To decrease the onset potential and preclude self-reduction, we introduce a Ga_2O_3 thin layer as a buffer layer between the Cu_2O sunlight absorber layer and the TiO_2 protective layer. This buffer layer decreases the conduction band discontinuity at the Cu_2O/buffer layer interface and thus increases the photovoltage of the structure, thus improving the efficiency and the stability. The fabricated Pt/TiO_2/Ga_2O_3/Cu_2O structure achieves a large shift of the onset potential toward positive values and a stable photocurrent over at least two hours. The observed onset potential of 1.02 V *vs.* RHE and the large photocurrent generated at low applied biases demonstrate the potential of this structure for developing superior photoelectrodes for use in high-efficiency tandem cells.

In recent decades, the booming energy demand in modern industrial development has speeded up the consumption of conventional energy sources such as coal and oil; thus, the usage of clean and renewable energy sources to avoid energy shortages and serious environmental concerns associated with fossil fuel combustion have gained extensive attention. Hydrogen is considered to be an environmentally friendly fuel for the future, and the photoelectrochemical (PEC) water splitting system provides a promising process to produce hydrogen from water by sustainable solar energy at the semiconductor/electrolyte interface.[1–9] Although considerable research into solar water splitting has been developed within the past decade, the construction of stable and efficient photoelectrodes to achieve a solar-to-hydrogen (STH) conversion efficiency of more than 10% required for practical applications is still challenging.[10–15] In this view, the use of a single photoanode in tandem with a single photocathode to achieve a more efficient PEC system without the need for external voltage is strongly desired. However, the STH conversion efficiency of this kind of tandem cell is still not high (below 0.5%),[16–21] which can be mainly attributed to the small photovoltages, resulting in large external voltage to drive the water splitting reaction on the electrodes. Therefore, developing highly active photoelectrodes working with small applied voltage for efficient PEC water splitting is desired.

[a] *School of Engineering, The University of Tokyo, 7-3-1 Hongo, Bunkyo-ku, Tokyo 113-8656, Japan. E-mail: jean@mech.t.u-tokyo.ac.jp*
[b] *Department of Chemical System Engineering, The University of Tokyo, 7-3-1 Hongo, Bunkyo-ku, Tokyo 113-8656, Japan*
[c] *Institute of Engineering Innovation, The University of Tokyo, 2-11-16, Yayoi, Bunkyo-ku, Tokyo 113-8656, Japan*

† Electronic supplementary information (ESI) available. See DOI: 10.1039/c5ee00250h

One of the materials of choice is Cu_2O, a p-type semiconductor with a direct band gap of 2.0 eV, which can function as a photocathode that enables effective utilization of solar photons. The theoretical maximum STH conversion efficiency of 18.1% and the corresponding photocurrent of -14.7 mA cm^{-2} based on the air mass 1.5 global (AM 1.5G) spectrum make it a very promising semiconductor for hydrogen production.[9] However, Cu_2O can be easily reduced into Cu in solution under illumination and bias, which limits the use of this material in photocatalytic water splitting. To address this problem, a suitable protective layer with a favorable energy band position on bare Cu_2O is essential for a stable and efficient water splitting reaction instead of Cu_2O self-reduction. It has been reported recently that the TiO_2 layer can serve as an excellent protective layer for unstable photoelectrodes as well as reducing the impediment for electron transfer under PEC hydrogen evolution conditions.[9,22–26] Pioneering studies have shown that the TiO_2-protected Cu_2O-based photocathodes exhibit a large photocurrent and enhanced stability performance when using ZnO as a buffer layer.[9,24–26] However, a relatively negative onset potential (0.45–0.55 V *vs.* RHE) was obtained in this structure, which is related to the small photovoltage produced by the heterojunctions. A recent work shows that the introduction of a ZnS buffer layer between the Cu_2O and TiO_2 can shift the onset potential cathodically to some extent (0.72 V *vs.* RHE) by increasing the photovoltage at multilayer/electrolyte junctions.[27] Therefore, a rational adjustment of the buffer layer is expected to increase the photovoltage further by forming a better energy band alignment across the multilayers.

Here, we introduce a Ga_2O_3 thin layer as a very suitable buffer layer between the Cu_2O layer and the TiO_2 protective layer to achieve a higher photovoltage and stable photocurrent. The Ga_2O_3 layer provides an approximately equal electron affinity to that of Cu_2O, thus decreasing the height of the conduction band discontinuity at the Ga_2O_3/Cu_2O interface and likely reducing the interfacial recombination.[28,29] The stabilization of the photocathode is realized by first coating a conformal TiO_2 thin film and then depositing a thin Pt layer to promote PEC hydrogen production. A systematic investigation of the effect of TiO_2 deposition temperature on the performance of the photocathode indicates that an optimized energy band alignment can be achieved at a deposition temperature of 220 °C, at which a high photocurrent of -2.95 mA cm^{-2} at 0 V *vs.* RHE and an extremely low onset potential of 1.02 V *vs.* RHE are observed. The enhanced photocathodic performance observed at low applied biases (-1.17 mA cm^{-2} at 0.6 V *vs.* RHE) demonstrates the great potential of this structure for developing superior photoelectrodes for use in tandem cells.

Experimental section

Fabrication of Cu_2O microcrystalline films

The Cu_2O microcrystalline film was prepared by a two-step fabrication method. This method consists of the synthesis of $Cu(OH)_2$ nanowires and their subsequent transformation into Cu_2O at 500 °C under vacuum. First, a Cu foil (99.96%, Nilaco) with a size of 10 × 30 mm^2 and a thickness of 0.2 mm was cleaned in ultrasonic bath of acetone and ethanol for 10 min, sequentially. The cleaned Cu foil was then immersed into a mixed solution of 2.67 M NaOH (97.0%, Wako) and 0.133 M $(NH_4)_2S_2O_8$ (98.0%, Wako) for 10 min. In addition, gentle stirring of the solution at low temperature (5 °C) was introduced to prevent the growth of CuO microflower structures on the $Cu(OH)_2$ nanowires. CuO microflowers were found to grow under the conditions of inhomogeneous solution and increased temperature near the Cu/solution interface caused by the chemical reaction. Finally, the Cu foil covered by a $Cu(OH)_2$ nanowire with a light blue color was taken out from the solution, rinsed with deionized water, and dried in air. To synthesize the Cu_2O film, the obtained $Cu(OH)_2$ nanowires/Cu foil was loaded into an alumina boat and placed at the center of a vacuum quartz tube. The quartz tube was evacuated to about 36 Pa before heating under a flow rate of Ar of 50 sccm. The working pressure during the annealing was kept at about 2.5 × 10^3 Pa. The Cu_2O microcrystalline layers were prepared by annealing the $Cu(OH)_2$ nanowire film at 500 °C for 2 h.

Atomic layer deposition of Ga_2O_3 and TiO_2 thin films

Before the deposition of oxide films, the Cu_2O film was treated by Ar plasma in a reactive ion etching (RIE) system (SAMCO, RIE-10NRU) for 30 s at room temperature to remove the residual contaminants from the annealing and change the hydrophobic surface to a hydrophilic surface. The Ar plasma was generated under an applied RF power of 50 W, a gas flow of 50 sccm and a pressure of 25 Pa. A Ga_2O_3 buffer layer and a TiO_2 protective layer were deposited on the surface of the Cu_2O microcrystalline layers with an ALD system (SUGA, SAL100H). The Ga_2O_3 layer was deposited at a substrate temperature of 150 °C using tris(dimethylamido)gallium (Aldrich, 98%, $T_{precursor}$ = 130 °C) and H_2O as Ga and O sources, respectively. TiO_2 was deposited using tetrakis(dimethylamido)titanium (Aldrich, 99.999%, $T_{precursor}$ = 90 °C) and H_2O as the Ti and O precursors, respectively. The substrate temperature of TiO_2 deposition was varied between 120 and 260 °C in order to control the quality of the deposited oxide films. For comparison, a ZnO buffer layer was also deposited on Cu_2O to fabricate $TiO_2/ZnO/Cu_2O$ structure by using diethylzinc (Japan Advanced Chemicals, $T_{precursor}$ = room temperature) as a Zn source, with a substrate temperature of 150 °C. The cycle numbers for TiO_2, Ga_2O_3 and ZnO are 220, 200 and 106, respectively.

Cocatalyst deposition

Platinum nanoparticles were deposited on the surface of the protective layer/Cu_2O samples by ion-beam sputtering of a Pt target to enhance the kinetics of the hydrogen production reaction. The chamber pressure was evacuated to 4 × 10^{-5} Pa before sputtering and, the substrate holder was at a distance of 22 cm from the Pt target. The Ar flow was adjusted to get a gas pressure of 3 × 10^{-2} Pa. The Ar ion beam had an energy of 1.5 keV and a diameter of 30 mm. The thickness of the Pt layer was monitored using a quartz crystal monitor and a thickness of 1 nm (nominally) was obtained after sputtering.

PEC measurements

The PEC performance of the protective layer/Cu_2O electrodes was performed in a three-electrode configuration using a Ag/AgCl reference electrode and a Pt wire counter electrode. The electrolyte was a 0.5 M Na_2SO_4–0.1 M KH_2PO_4 solution with a pH of 4.26. The measured potential *vs.* Ag/AgCl was converted to RHE by Nernst's equation ($E_{RHE} = E_{Ag/AgCl} + 0.059\ pH + 0.197$). The electrolyte was stirred and purged with argon gas before each measurement (for 15 min) and during measurements. The current–potential curves were measured both under 500 W Xe lamp illumination (286 mW cm^{-2}) and AM 1.5G simulated sunlight (100 mW cm^{-2}). The scan rate for the linear sweep voltammetry was 10 mV s^{-1}. To calculate the solar energy conversion efficiency (η), the equation $\eta = (V_{app} \times J_{ph})/P \times 100\%$ was used, where V_{app} is the applied potential (*vs.* RHE), J_{ph} is the photocurrent (mA cm^{-2}) under AM 1.5G irradiation and P is the irradiance of the AM 1.5G (100 mW cm^{-2}). The wavelength dependence of IPCE was measured under monochromatic irradiation using the 500 W Xe lamp equipped with bandpass filters (central wavelengths of 350, 400, 450, 500, and 550 nm). The IPCE at each wavelength was calculated according to the equation $IPCE\% = [J_{ph}(mA\ cm^{-2}) \times 1240]/[P(mW\ cm^{-2}) \times \lambda(nm)] \times 100$.

Structural characterization

The morphology of the samples was characterized using a field-emission scanning electron microscope (JEOL JSM 7600FA). The X-ray diffraction (XRD) patterns were determined using a diffractometer (SmartLab, Rigaku Co. Ltd, Japan) with Cu Kα radiation (1.540598 Å). XPS data were collected using a PHI 5000 VersaProbe (ULVAC-PHI) with an Al Kα X-ray source (1486.6 eV). The UV-vis diffuse reflectance spectra were using with a spectrophotometer equipped with an integrating sphere (DRS, V-560, Jasco). The structure of the sample was also identified by scanning transmission electron microscopy (STEM) and energy dispersive X-ray spectroscopy (EDS), with a JEM-2800, JEOL. The cross section was prepared by focused ion beam using an FIB-SEM (JIB-4600F, JEOL) and subsequent milling in a NanoMill 1040, E.A. Fischione Instruments.

Results and discussion

Characterization of the $TiO_2/Ga_2O_3/Cu_2O$ structures

Cu_2O microcrystalline films were prepared on Cu foil by a two-step fabrication method, as reported previously.[30] The $Cu(OH)_2$ nanowires were used as a template for growth of highly photoactive Cu_2O film with large surface area. Briefly, the $Cu(OH)_2$ nanowires on a Cu foil were fabricated by a wet chemical process in sodium hydroxide and ammonium solution, then the $Cu(OH)_2$ nanowire/Cu foils were annealed under an Ar atmosphere at 500 °C for 2 h. During the annealing, the $Cu(OH)_2$ nanowires were decomposed to CuO nanowires at about 120 °C, and the subsequent oxide growth was driven by outward diffusion of Cu ions *via* Cu vacancies from the Cu substrate to the oxide surface and a reaction with oxygen from the gas phase. The continuous diffusion of Cu ions on the surface of nanowires leads to volume expansion of the nanowires and consequently coalescence of the nanowires to form larger Cu_2O crystals. The obtained Cu_2O film consists of dense micro-nano aggregates with a diameter and length of ~0.6 and ~3.5 μm, respectively, as shown in Fig. S1a (ESI†). Fig. 1a shows the top morphology of the Cu_2O microcrystalline film after coating 20 nm of Ga_2O_3(150 °C) and 15 nm of TiO_2(220 °C). No obvious change in the morphology of the microcrystals was found because the coating was homogeneous. XRD measurements revealed only Cu_2O and Cu diffraction peaks from the TiO_2(15 nm)/Ga_2O_3(20 nm)/Cu_2O sample (Fig. S3a, ESI†). The absence of Ga_2O_3 and TiO_2 signals may be due to the thin thickness and low crystallinity of the oxide layers. In order to characterize the chemical state of the overlayers, XPS was conducted on the Ga_2O_3/Cu_2O and $TiO_2/Ga_2O_3/Cu_2O$ samples. With a very thin layer of Ga_2O_3(2 nm) on Cu_2O, the XPS spectrum showed the Ga 2p (1118.0 and 1144.9 eV) and

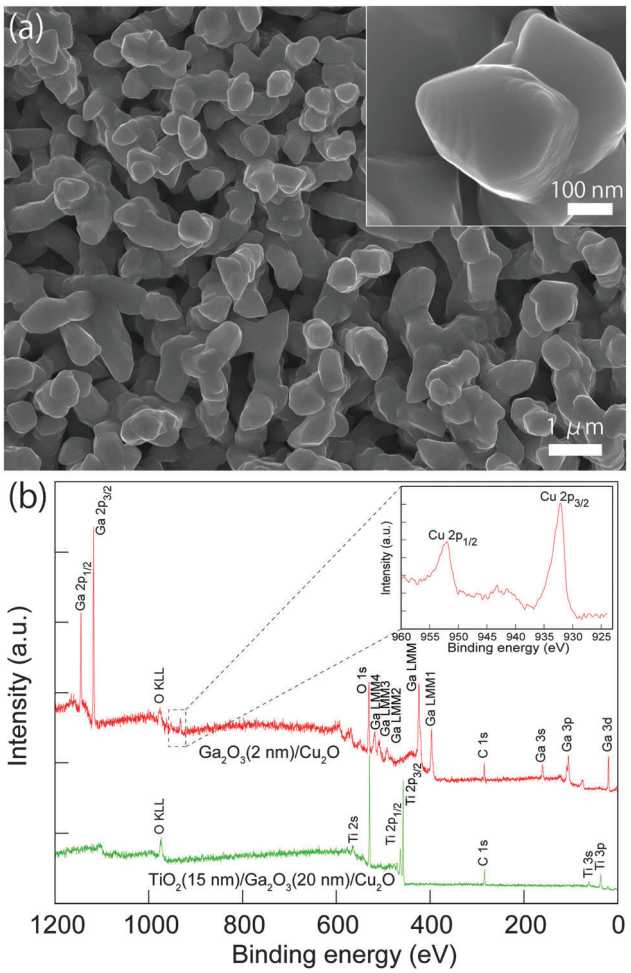

Fig. 1 (a) FE-SEM images of Cu_2O microcrystalline film coated with a Ga_2O_3 buffer layer and a TiO_2 protective layer by atomic layer deposition. (b) XPS spectra of Ga_2O_3(2 nm)/Cu_2O and TiO_2(15 nm)/Ga_2O_3(20 nm)/Cu_2O samples. Deposition temperature for Ga_2O_3 and TiO_2 are 150 and 220 °C, respectively. Top right inset is the high resolution XPS spectrum of Cu-2p peaks of the Ga_2O_3(2 nm)/Cu_2O sample.

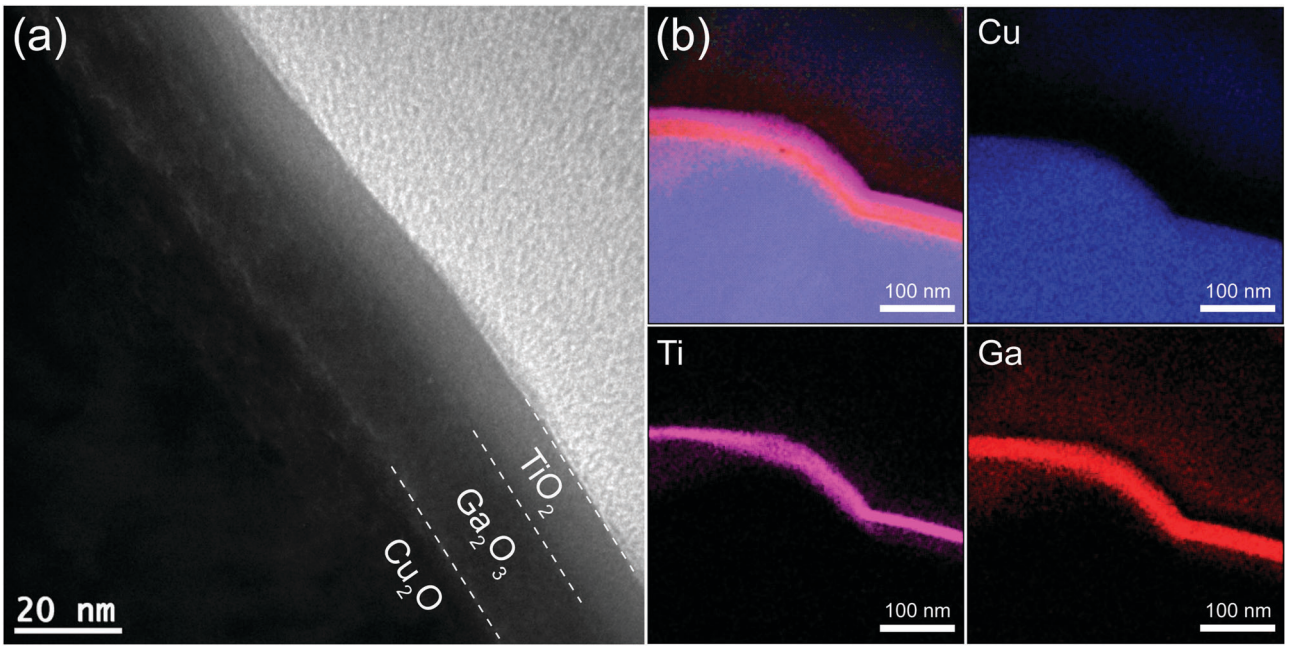

Fig. 2 (a) Typical cross-sectional TEM image of the TiO_2(15 nm)/Ga_2O_3(20 nm)/Cu_2O structure. (b) STEM-EDX mapping results of the structure. Deposition temperature for Ga_2O_3 and TiO_2 are 150 and 220 °C, respectively.

O 1s (530.4 eV) peaks for Ga_2O_3. In addition, Cu 2p peaks from the Cu_2O underlayer are also observed. The Cu_2O layer showed two main peaks at 932.2 and 952.1 eV corresponding to the $2p_{3/2}$ and $2p_{1/2}$ levels of Cu_2O. The shoulder peak at 933.7 eV and broad satellite peaks between 940 and 945 eV can be attributed to the thin CuO layer that is present on Cu_2O from natural oxidation. For the $TiO_2/Ga_2O_3/Cu_2O$ sample, the presence of Ti peaks and the absence of Ga and Cu peaks indicate that the ALD-deposited TiO_2 layer fully covered the Ga_2O_3, as indicated in Fig. 1b and Fig. S3b (ESI†). Fig. 2a shows a cross-section transmission electron microscopy (TEM) image of the TiO_2(220 °C)/Ga_2O_3(150 °C)/Cu_2O structure. It is found that both the Ga_2O_3 and TiO_2 layers are amorphous and the interfaces between Ga_2O_3/Cu_2O and TiO_2/Cu_2O are of high quality. The mapping of the elements for the cross-section sample reveals a homogeneous deposition of the oxide layers, as shown in Fig. 2b. Images of the large-area element mapping presented in Fig. S4 (ESI†) also confirm the homogeneous deposition. From the TEM analysis, the thicknesses of TiO_2 and Ga_2O_3 are both estimated to be 15–20 nm. The uniform coating of the TiO_2 overlayer enables an effective protection for the Cu_2O layer against the solution corrosion.

PEC properties of $Pt/TiO_2/Ga_2O_3/Cu_2O$ photocathodes

In the PEC characterization, the bare Cu_2O electrode exhibited a large photocathodic current and negative onset voltage under visible light (>420 nm) illumination, however, this photocurrent decreased significantly in the beginning of the stability test. The electrode almost lost its photoactivity after 20 min of continuous illumination at 0 V *vs.* RHE (Fig. S5, ESI†). The instability of the Cu_2O electrode is consistent with the previous reports,[9,30] and can be attributed to the reduction of Cu_2O to Cu under illumination and bias potential. Thus, the n-type protective layer coating is expected to improve the stability of Cu_2O. Besides, the buried junction formed between the p-type Cu_2O and the n-type oxide layer can also generate a photovoltage to shift the onset voltage positively. Fig. 3a shows the current–potential curves for the $Pt/TiO_2/Ga_2O_3/Cu_2O$ electrodes measured under a 500 W Xe lamp. The Ga_2O_3 buffer layer was deposited under the same conditions (20 nm, 150 °C) for all the electrodes, while the deposition temperature of TiO_2 was varied from 120 to 260 °C to investigate the effect of TiO_2 quality on the performance of the electrode. The 120 °C-deposited TiO_2 sample yielded a relatively low photocurrent and negative onset voltage. When the TiO_2 deposition temperature increased to 150, 180, and 220 °C, the photocurrent of the electrodes increased significantly, with an enhancement factor of ~2.60, ~3.46, and ~6.30 compared to the photocurrent obtained with the 120 °C-deposited electrode, respectively. Moreover, the onset voltage of the electrodes shifts positively with increasing TiO_2 deposition temperature, so that an extremely positive onset potential of around 1 V *vs.* RHE was achieved with the samples prepared at 180 and 220 °C. The pronounced photocathodic current and the positive onset potential can contribute to the improvement of the overall efficiency, which will be presented and discussed later in accordance with the data obtained under AM 1.5G illumination. The enhancement in both the photocurrent and the onset potential is most likely related to improved crystallinity of TiO_2 and alignment of the energy bands occurring at higher TiO_2 deposition temperatures. When the temperature increased to 260 °C, a dramatic decrease in the photocurrent was observed.

To further clarify the high PEC performance achieved for the TiO_2 deposition temperature of 220 °C, the line profiles for Ti,

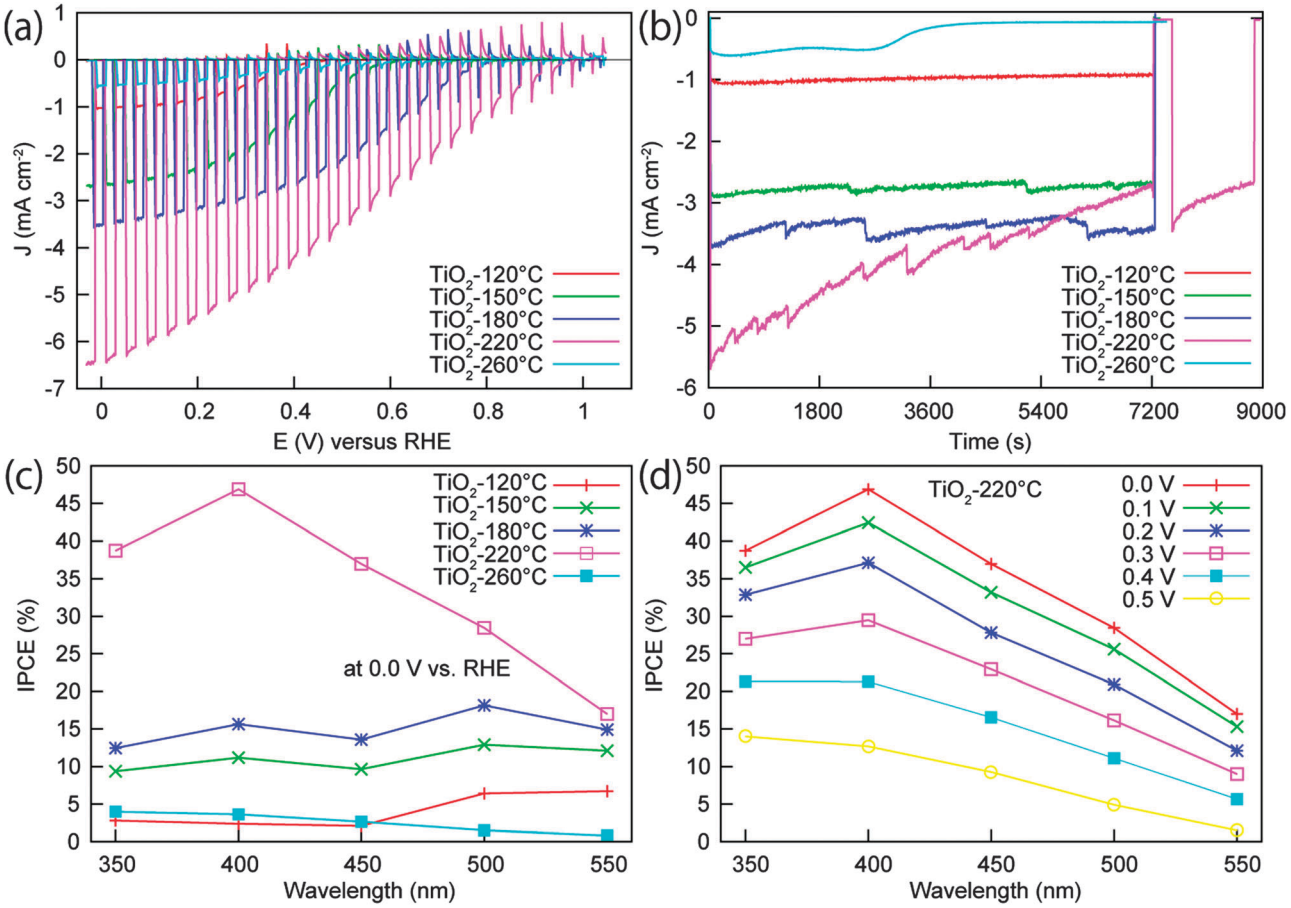

Fig. 3 (a) Current–potential curves and (b) current–time curves (held at 0 V *vs.* RHE) of Pt/TiO_2/Ga_2O_3/Cu_2O samples with different TiO_2 deposition temperatures. Deposition temperature for Ga_2O_3 is kept at 150 °C. (c) Wavelength dependence of IPCE measured at 0 V *vs.* RHE for those samples. (d) Wavelength dependence of IPCE for Pt/TiO_2/Ga_2O_3/Cu_2O electrodes with TiO_2 deposition temperature of 220 °C at different applied potentials (*vs.* RHE). Curves were measured in 0.5 M Na_2SO_4–0.1 M KH_2PO_4 solution (pH = 4.26) under 500 W Xe lamp.

Ga, and Cu elements across the TiO_2(220 °C)/Ga_2O_3(150 °C)/Cu_2O interface were measured (Fig. S6, ESI†). The result shows a moderate diffusion of Ga in Cu_2O for this sample. The observed amorphousness of the ALD deposited materials does not suggest the formation of a different crystalline phase at the interfaces. Additionally, the reflectance spectra (Fig. S7, ESI†) for the TiO_2/Ga_2O_3/Cu_2O samples show a large decrease in the absorption edge of Cu_2O for a TiO_2 deposition temperature of 220 °C. Thus, combining the TEM-EDX element line analysis and the reflectance spectra data, we conclude that Ga diffusion in Cu_2O occurred at 220 °C and the ion diffusion may have contributed to improve the interface quality and electron transport. Recently, a similar Cd diffusion in $CuGa_3Se_5$ at the CdS/$CuGa_3Se_5$ interface was reported by Zhang *et al.*[31] The Cd diffusion and the associated excellent PEC performance of this photocathode (CdS/$CuGa_3Se_5$/ACGSe) indicate that a moderate diffusion of ions from the overlayer into the Cu-deficient p-type semiconductor can favour the electron transport. With a higher temperatures of 260 °C, the disappearance of the absorption edge of Cu_2O (Fig. S7, ESI†) suggests enhanced Ga diffusion at this high temperature, which may result in the formation of a $CuGaO_2$ thin layer due to the Ga overdiffusion. Considering that the conduction band of p-type $CuGaO_2$ (~−2.5 V *vs.* RHE)[32,33] is much more negative than that of the Cu_2O conduction band (~−1.23 V *vs.* RHE),[30] the $CuGaO_2$/Cu_2O interface is not favourable for electron transport because of the presence of a large conduction band offset (~1.27 eV) and energy barrier at the interface. Thus, the observed drastic decrease in the PEC performance at 260 °C may be explained by the over-diffusion of Ga under high deposition temperature.

To determine the stability of Pt/TiO_2/Ga_2O_3/Cu_2O photoelectrodes, the time dependency of the photocurrent was tested at 0 V *vs.* RHE under 500 W Xe lamp irradiation as shown in Fig. 3b. The photocathodes fabricated with TiO_2 deposition temperatures of 120, 150, and 180 °C maintained a highly stable photocurrent for 2 h, during which the fluctuation in the photocurrent was caused by the formation and detachment of H_2 bubbles, as presented in Fig. S8b and c (ESI†). The SEM characterization for the 180 °C-deposited sample after a 2 h stability test indicates that no obvious morphology change occured during the stability test (Fig. S9, ESI†). Furthermore, the presence of Ti and Pt peaks and the absence of Ga peaks in the XPS spectrum reveal that the photocathode is stable against corrosion in the electrolyte, as shown in Fig. S9e (ESI†). For the 220 °C-deposited electrode, the

sample showed a large photocurrent, but the current decreased slowly with time. After the 2 h test and a following short rest, 60% of the initial photocurrent was obtained. With the deposition temperature of 260 °C, the photocurrent was low and could only be maintained for about 50 min, the photocathode losing its activity after one-hour stability test. The decay of the photocurrent for the electrodes prepared above 220 °C may be attributed to the degradation of the TiO_2 layer and/or the detachment of Pt owing to H_2 bubble generation during the stability test.[9,24,25]

The wavelength dependency of the incident photon-to-current conversion efficiency (IPCE) for $Pt/TiO_2/Ga_2O_3/Cu_2O$ electrodes with different TiO_2 deposition temperatures are shown in Fig. 3c. The 220 °C-deposited sample exhibited the highest IPCE among the samples. At 0 V *vs.* RHE, the IPCEs for the Pt/TiO_2(220 °C)$/Ga_2O_3/Cu_2O$ electrode were above 36% in the 350–450 nm range. The maximum IPCE achieved was 46.9% at 400 nm. By decreasing the TiO_2 deposition temperature, the IPCE decreased correspondingly. Notably, at wavelengths below 450 nm, the electrodes with the TiO_2 deposition temperature equal to or lower than 180 °C showed much lower efficiency than the 220 °C-deposited one. The wavelength dependence of IPCE for the electrodes was not consistent with the absorbance spectrum of the samples (Fig. S7, ESI†). This may be ascribed to the complexity of the transport of photocarriers through the multilayers in this structure since the improvement in the conversion efficiency is dependent on not only the absorption of the incident photons but also the transmission of photocarriers to reach the surface for the chemical reaction. One possible reason for the efficiency loss with the TiO_2 layer prepared under the low temperatures is the low crystallinity and defective interfaces at the buffer layer interface resulting in high recombination rates. In contrast to the high IPCEs for the 220 °C-deposited sample, the IPCEs for the sample prepared at 260 °C were very low. The low performance can be attributed to the degradation of the Ga_2O_3/Cu_2O interface due to the overdiffusion of Ga into Cu_2O. The wavelength dependence of IPCE at different potentials (from 0.0 to 0.5 V *vs.* RHE) for the 220 °C-deposited sample was also investigated (Fig. 3d). The result indicates that even at the low applied potential of 0.5 V *vs.* RHE, the IPCEs are still relatively high, which is consistent with the high photocurrent at low potential presented in the current–potential curve.

The PEC water splitting properties of the photocathodes under AM 1.5G-simulated sunlight (100 mW cm^{-2}) are also given for comparison in Fig. 4a. The electrodes showed a large photocurrent under light and negligible current under dark conditions. The photocurrent densities of −0.54, −1.29, −1.64, and −2.95 mA cm^{-2} were obtained at 0 V *vs.* RHE (the voltage is swept from negative to positive) for the TiO_2 deposition temperatures of 120, 150, 180, and 220 °C, respectively. Interestingly, the onset potential of the Pt/TiO_2(220 °C)$/Ga_2O_3/Cu_2O$ electrode, defined as the potential at which a photocathodic current exceeds 20 μA cm^{-2}, was 1.02 V *vs.* RHE. This is superior to the onset potential of 0.96, 0.94, and 0.65 V *vs.* RHE obtained for 180, 150 and 120 °C-deposited samples. The onset potential in this report shows a significant enhancement over the previously-reported Cu_2O-based photocathodes, including the $TiO_2/ZnO/Cu_2O$(0.45–0.55 V),[24–26] carbon/Cu_2O(0.6 V),[34] and $TiO_2/ZnS/Cu_2O$(0.72 V)[27] structures. The best electrode (220 °C) shows an exceptional photocathodic current at positive potential, *i.e.*, −1.17 mA cm^{-2} at 0.6 V *vs.* RHE, which makes it a promising candidate for tandem cell applications. Fig. 4b shows the solar energy conversion efficiency of the electrodes calculated from the current–potential curves of Fig. 4a. A maximum conversion efficiency of 0.16, 0.40, 0.58, and 0.78% was achieved at 0.38, 0.43, 0.56, and 0.45 V *vs.* RHE for the 120, 150, 180 and 220 °C-deposited electrodes, respectively.

Band alignments of heterojunctions

To investigate the effect of the buffer layers on the performance of Cu_2O-based photocathodes, the band alignment of the buffer layer/Cu_2O interface was calculated by photoelectron spectroscopy according to the method outlined by Waldrop *et al.*[29,35–38]

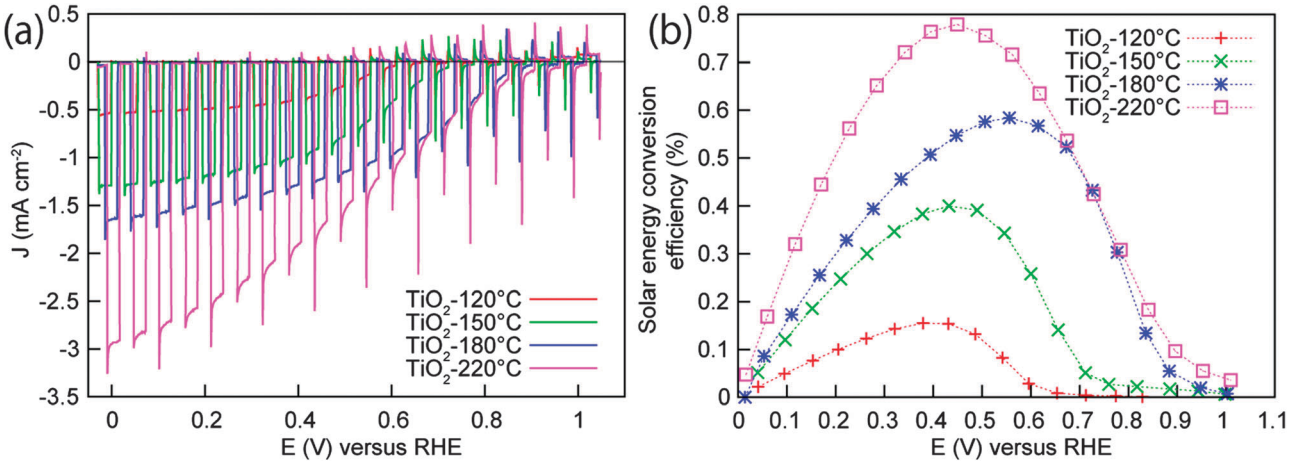

Fig. 4 (a) Current–potential curves for $Pt/TiO_2/Ga_2O_3/Cu_2O$ photocathode obtained for different TiO_2 deposition temperatures under AM 1.5 G irradiation at 100 mW cm^{-2}. Curves were measured in 0.5 M Na_2SO_4–0.1 M KH_2PO_4 solution (pH = 4.26), and potential was swept in positive direction at a rate of 10 mV s^{-1}. (b) Solar energy conversion efficiency of photocathodes calculated from current–potential curves in (a).

The offset of E_{CBM} between Cu_2O and Ga_2O_3 was determined to be in the range between −0.37 and +0.01 eV (Fig. S2, ESI†), indicating the approximately equal electron affinity of the Cu_2O and Ga_2O_3 layers. Thus, the introduction of the Ga_2O_3 buffer layer decreases the conduction band discontinuity at the Cu_2O/Ga_2O_3 interface, which is known to improve the open circuit voltage and the fill factor of solar cells by reducing recombination.[28,29] In the PEC hydrogen evolution on Cu_2O-based photocathodes, this is reflected in the cathodic shift in the onset potential of the photocurrent. In addition, the use of a Ga_2O_3 thin layer allows to grow TiO_2 buffer layers at higher temperatures owing to its high thermal resistance. The reported decrease in the onset potential with the TiO_2 deposition temperature is ascribed to an improved Cu_2O/Ga_2O_3 and Ga_2O_3/TiO_2 interfaces formed under high temperature deposition of the TiO_2 layer. For comparison purposes, a ZnO buffer layer with an electron affinity much higher than that of Cu_2O was used to fabricate a $TiO_2/ZnO/Cu_2O$ photocathode. As shown in Fig. S11 (ESI†), the obtained $Pt/TiO_2/ZnO/Cu_2O$ photocathodes exhibited a much more negative onset potential (lower photovoltage) than the $Pt/TiO_2/Ga_2O_3/Cu_2O$ photocathodes, indicative of the large conduction band discontinuity between ZnO and Cu_2O.[9,24] To confirm this result, the same photoelectron spectroscopy method was used to characterize the band alignment between ZnO/Cu_2O interface. The ZnO/Cu_2O heterojuntion actually possesses a large conduction band offset in the range from −1.56 to −1.42 eV (Fig. S12, ESI†), similar to previous reports.[36–38] Moreover, the $TiO_2/ZnO/Cu_2O$ electrode prepared with a TiO_2 deposition temperature of 220 °C shows a decreased photocurrent. This is due to the overdiffusion of ions at the buffer layer/Cu_2O interface, similar to the case of $TiO_2/Ga_2O_3/Cu_2O$ treated at 260 °C. In conclusion, the Ga_2O_3 thin layer, owing to its high thermal resistance, worked as a suitable buffer layer to grow TiO_2 layers with improved quality. Thus the obtained large energy gap between the p-type absorber and the n-type overlayers inhibits the interface recombination and provides a large driving force for the transport of photogenerated electrons in the photocathode, resulting in efficient H_2 reduction on the surface with the assistance of the Pt co-catalyst.

Conclusions

We have successfully deposited a Ga_2O_3 thin film as an appropriate buffer layer for improving the performance of TiO_2-coated Cu_2O-based photocathodes. The Ga_2O_3 buffer layer provided an electron affinity approximately equal to that of Cu_2O, thus decreasing the conduction band discontinuity along the Cu_2O/Ga_2O_3 interface. In addition, high thermal resistance of Ga_2O_3 allowed for ALD of TiO_2 at relatively high temperatures. These factors enabled suppression of the interface recombination and improvement in the photovoltage. An extremely positive onset voltage of 1.02 V *vs.* RHE was achieved by tuning the TiO_2 deposition temperature to 220 °C. The photocathode produced a photocurrent of -2.95 mA cm^{-2} at 0 V *vs.* RHE with a conversion efficiency of 0.78% at 0.45 V *vs.* RHE under AM 1.5G illumination. Moreover, the photocathodes exhibited a stable photocurrent under continuous illumination for 2 h for the deposition temperatures of TiO_2 ranging from 120 to 180 °C, providing a promising photocathode candidate for high performance tandem cells.

Acknowledgements

The XRD analysis, electron microscopy, and EDX mapping were conducted in the Research Hub for Advanced Nano Characterization, The University of Tokyo, supported by the Ministry of Education, Culture, Sports, Science and Technology (MEXT), Japan. Part of this work was supported by the JSPS Core-to-Core program (Advanced Research Networks type A) and Grants-in-Aids for Specially Promoted Research (No. 23000009) and for Young Scientists (B) (No. 25810112). The authors thank Prof. Yuichi Ikuhara of The University of Tokyo for his assistance in the electron microscopy and the EDX mapping. C.L. thanks the China Scholarship Council (201206230077).

Notes and references

1 A. Fujishima and K. Honda, *Nature*, 1972, **238**, 37.
2 O. Khaselev and J. A. Turner, *Science*, 1998, **280**, 425.
3 R. Asahi, T. Morikawa, T. Ohwaki, K. Aoki and Y. Taga, *Science*, 2001, **293**, 269.
4 Z. G. Zou, J. H. Ye, K. Sayama and H. Arakawa, *Nature*, 2001, **414**, 625.
5 K. Maeda, T. Takata, M. Hara, N. Saito, Y. Inoue, H. Kobayashi and K. Domen, *J. Am. Chem. Soc.*, 2005, **127**, 8286.
6 I. Cesar, A. Kay, J. A. Gonzalez Martinez and M. Grätzel, *J. Am. Chem. Soc.*, 2006, **128**, 4582.
7 T. Hisatomi, H. Dotan, M. Stefik, K. Sivula, A. Rothschild, M. Grätzel and N. Mathews, *Adv. Mater.*, 2012, **24**, 2699.
8 S. W. Boettcher, E. L. Warren, M. C. Putnam, E. A. Santori, D. Turner-Evans, M. D. Kelzenberg, M. G. Walter, J. R. McKone, B. S. Brunschwig, H. A. Atwater and N. S. Lewis, *J. Am. Chem. Soc.*, 2011, **133**, 1216.
9 A. Paracchino, V. Laporte, K. Sivula, M. Grätzel and E. Thimsen, *Nat. Mater.*, 2011, **10**, 456.
10 X. B. Chen, L. Liu, P. Y. Yu and S. S. Mao, *Science*, 2011, **331**, 746.
11 Y. B. Li, L. Zhang, A. Torres-Pardo, J. M. González-Calbet, Y. H. Ma, P. Oleynikov, O. Terasaki, S. Asahina, M. Shima, D. K. Cha, L. Zhao, K. Takanabe, J. Kubota and K. Domen, *Nat. Commun.*, 2013, **4**, 2566.
12 Q. H. Liu, J. F. He, T. Yao, Z. H. Sun, W. R. Cheng, S. He, Y. Xie, Y. H. Peng, H. Cheng, Y. F. Sun, Y. Jiang, F. C. Hu, Z. Xie, W. S. Yan, Z. Y. Pan, Z. Y. Wu and S. Q. Wei, *Nat. Commun.*, 2014, **5**, 5122.
13 M. Moriya, T. Minegishi, H. Kumagai, M. Katayama, J. Kubota and K. Domen, *J. Am. Chem. Soc.*, 2013, **135**, 3733.
14 T. W. Kim and K. S. Choi, *Science*, 2014, **343**, 990.

15 C. Liu, J. Y. Tang, H. M. Chen, B. Liu and P. D. Yang, *Nano Lett.*, 2013, **13**, 2989.
16 W. B. Ingler and S. U. M. Khan, *Electrochem. Solid-State Lett.*, 2006, **9**, G144.
17 H. L. Wang, T. Deutsch and J. A. Turner, *J. Electrochem. Soc.*, 2008, **155**, F91.
18 S. Ida, K. Yamada, T. Matsunaga, H. Hagiwara, Y. Matsumoto and T. Ishihara, *J. Am. Chem. Soc.*, 2010, **132**, 17343.
19 Q. X. Jia, K. Iwashina and A. Kudoa, *Proc. Natl. Acad. Sci. U. S. A.*, 2012, **109**, 11564.
20 Q. P. Chen, J. H. Li, X. J. Li, K. Huang, B. X. Zhou and W. F. Shangguan, *ChemSusChem*, 2013, **6**, 1276.
21 P. Bornoz, F. F. Abdi, S. D. Tilley, B. Dam, R. van de Krol, M. Graetzel and K. Sivula, *J. Phys. Chem. C*, 2014, **118**, 16959.
22 B. Seger, T. Pedersen, A. B. Laursen, P. C. K. Vesborg, O. Hansen and I. Chorkendorff, *J. Am. Chem. Soc.*, 2013, **135**, 1057.
23 S. Hu, M. R. Shaner, J. A. Beardslee, M. Lichterman, B. S. Brunschwig and N. S. Lewis, *Science*, 2014, **344**, 1005.
24 A. Paracchino, N. Mathews, T. Hisatomi, M. Stefik, S. D. Tilley and M. Grätzel, *Energy Environ. Sci.*, 2012, **5**, 8673.
25 S. D. Tilley, M. Schreier, J. Azevedo, M. Stefik and M. Grätzel, *Adv. Funct. Mater.*, 2014, **24**, 303.
26 C. G. Morales-Guio, S. D. Tilley, H. Vrubel, M. Grätzel and X. L. Hu, *Nat. Commun.*, 2013, **5**, 3059.
27 P. C. Dai, W. Li, J. Xie, Y. M. He, J. Thorne, G. McMahon, J. H. Zhan and D. W. Wang, *Angew. Chem.*, 2014, **126**, 1.
28 T. Minami, Y. Nishi and T. Miyata, *Appl. Phys. Express*, 2013, **6**, 044101.
29 Y. S. Lee, D. Chua, R. E. Brandt, S. C. Siah, J. V. Li, J. P. Mailoa, S. W. Lee, R. G. Gordon and T. Buonassisi, *Adv. Mater.*, 2014, **26**, 4704.
30 C. L. Li, Y. B. Li and J. J. Delaunay, *ACS Appl. Mater. Interfaces*, 2014, **6**, 480.
31 L. Zhang, T. Minegishi, M. Nakabayashi, Y. Suzuki, K. Seki, N. Shibata, J. Kubota and K. Domen, *Chem. Sci.*, 2015, **6**, 894.
32 A. Renaud, B. Chavillon, L. Le Pleux, Y. Pellegrin, E. Blart, M. Boujtita, T. Pauporté, L. Cario, S. Jobic and F. Odobel, *J. Mater. Chem.*, 2012, **22**, 14353.
33 K. Ueda, T. Hase, H. Yanagi, H. Kawazoe, H. Hosono, H. Ohta, M. Orita and M. Hirano, *J. Appl. Phys.*, 2001, **89**, 1790.
34 Z. H. Zhang, R. Dua, L. B. Zhang, H. B. Zhu, H. N. Zhang and P. Wang, *ACS Nano*, 2013, **7**, 1709.
35 J. R. Waldrop, R. W. Grant, S. P. Kowalczyk and E. A. Kraut, *J. Vac. Sci. Technol., A*, 1985, **3**, 835.
36 Y. S. Lee, J. Heo, S. C. Siah, J. P. Mailoa, R. E. Brandt, S. B. Kim, R. G. Gordon and T. Buonassisi, *Energy Environ. Sci.*, 2013, **6**, 2112.
37 L. M. Wong, S. Y. Chiam, J. Q. Huang, S. J. Wang, J. S. Pan and W. K. Chim, *J. Appl. Phys.*, 2010, **108**, 033702.
38 Z. Q. Duan, A. Du Pasquier, Y. C. Lu, Y. Xu and E. Garfunkel, *Sol. Energy Mater. Sol. Cells*, 2012, **96**, 292.